

# Evaluation of a Joint Hysteresis Model in a Robot Actuated by Pneumatic Muscles

Michael Kastner<sup>1</sup>, Hubert Gatringer<sup>1</sup> and Ronald Naderer<sup>2</sup>

<sup>1</sup>*Institute for Robotics, Johannes Kepler University Linz, Altenberger Strasse 69, 4040 Linz, Austria*

<sup>2</sup>*FerRobotics Compliant Robot Technology GmbH, Altenberger Strasse 69, 4040 Linz, Austria*

**Keywords:** Compliant Robotics, Pneumatic Muscles, Hysteresis Model.

**Abstract:** Passively compliant drives are interesting alternatives to classical stiff actuators in emerging fields like human-robot cooperation, service and rehabilitation robotics. Pneumatic muscles have been found to be interesting low-cost actuators for such purposes. To fully realize the (desired) higher sensitivity and at the same time maintain a good control quality, detailed models of the robot's own components are required. For pneumatic muscles, their hysteresis characteristic is a challenging property. In this paper we present a hysteresis model based on a Prandtl-Ishlinskii operator approach and evaluate the resulting performance when the inverse model is used for compensation in the position controller. The evaluation is done on a real multi-axes robot arm.

## 1 INTRODUCTION

Typical industrial robots are built as stiff as possible to ensure a high repeatability and tracking accuracy during free motion. For interaction tasks, the use of compliant robotic systems has long been researched. While this compliance is often added to standard robots by means of additional control algorithms and sensors, another approach is to use passively compliant drive technologies, i.e. actuators with a low natural stiffness. Compliant actuation systems have been and are actively researched for a large number of applications, including safe human/robot interaction for industrial or service robotics, contact processes, temporary energy storage, rehabilitation devices and walking robots.

One type of actuation that is particularly inspired by biological systems is the pneumatic muscle, which was originally used by McKibben for prosthesis applications. It consists of a rubber tube and an inelastic braided shell. When the tube is filled with pressurized air, the braid angle changes, causing a radial expansion and a longitudinal contraction. Two such muscles can be used in an antagonistic setup to create a prismatic or revolute joint. Because of the low cost of the muscle itself and the high forces it is able to exert, its use in robotics has also been investigated by several research groups.

Compared to pneumatic cylinders, the absence of a stick-slip effect helps with an accurate position con-

trol, but the actuator characteristic is still very complex and difficult to handle. Particularly, hysteresis causes disturbances every time the drive direction is reversed, while a creep/settling characteristic causes the actuation force to slowly drift after a maneuver.

In this paper we present a model for the hysteresis effect based on a Prandtl-Ishlinskii approach and discuss its use as a compensation term in the position controller of a pneumatically actuated industrial manipulator. Section 2 will detail the considered robot and joint setup. In Section 3 we will discuss advanced pneumatic muscle models that can be found in the literature and present our hysteresis model. The general control structure used and the incorporation of the hysteresis compensator are shown in Section 4, before measurement results from the real robot are presented in Section 5. Section 6 closes with conclusions and an outlook on planned activities.

## 2 SYSTEM SETUP

The robot system that we are dealing with in this contribution is an industrial robot arm manufactured by FerRobotics Compliant Robot Technology GmbH, called Romo (see Figure 1). It comprises seven rotational joints of which five are actuated pneumatically. The other two – used for longitudinal rotations – are driven by Schunk PowerCubes (electrically commu-

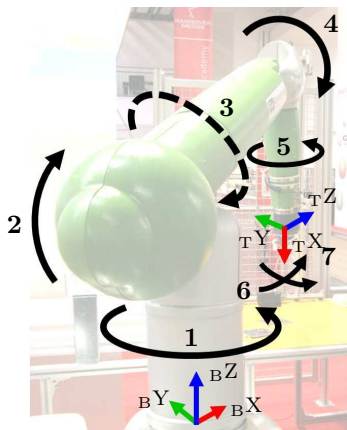


Figure 1: Considered robot Romo with joints 1 to 7 and tool (T) and base (B) coordinate systems.

tated motor modules). The three main joints (1, 2 and 4) are actuated by a pair of Festo DMSP-40 muscles each. Only these three joints will be considered in this paper. The basic joint principle is shown in Figure 2, the controller will be presented later (see Figure 6).  $q$  denotes the joint angle,  $Q$  the joint torque,  $F$  the muscle forces,  $p$  the muscle pressures and  $u$  the valve control voltages.

Each muscle pressure is measured by an according sensor located at the inlet, while the robot's original joint position instrumentation has been changed from cable extension sensors to optical encoders (17 bit, absolute) to improve the control performance. The muscles are actuated by Festo MPYE-18HF 5/3-way proportional directional slider valves. The control is implemented on an industrial PC with a realtime operating system (Bernecker and Rainer APC 620) with a Pentium M CPU clocked at 1.4 GHz. The controller cycle time is 0.5 ms. The Mathworks Realtime Workshop is used to generate C code for the PC from a Simulink implementation of the controller, much like on the well known dSpace rapid prototyping systems.

### 3 ADVANCED MUSCLE MODELING

Beyond the static contraction/pressure/force characteristic, several approaches for enhanced dynamical models of pneumatic muscles can be found in various publications. (Chou and Hannaford, 1994) observed that the braided pneumatic muscles they used showed a rate-independent hysteresis, which they attributed to Coulomb friction in the shell or between the shell and the bladder. They did not devise a mathematical model but tried to improve the situation using lubricants, which only led to small improvements. (Klute

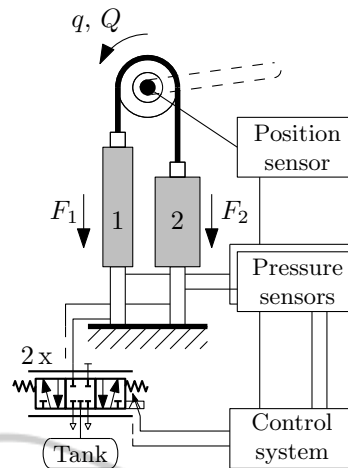


Figure 2: Concept drawing of a pneumatic joint.

et al., 2002) from the same research group compared the characteristic of the pneumatic artificial muscle to the famous Hill model for skeletal muscle, (Hill, 1938). Again, they found the pneumatic muscle to be very lightly damped and used an additional hydraulic damper to create a mechanical system that resembles the biological inspiration. The hysteresis effect is not mentioned in this article. (Reynolds et al., 2003) devise a model using spring and damper coefficients that are affine functions in the muscle pressure. (Kerscher et al., 2006) use a similar approach for modeling a Festo fluidic muscle. They evaluate their model in a quick-release setup inspired by Hill's experiments and conclude that the resulting force/velocity characteristic shows nearly the same curve progression as biological muscle. Around the same time (Toudu and Zagal, 2006) performed basically the same tests with custom braided muscles. They show that a version with a braided iron shell can be modeled with a constant viscous friction coefficient, while for a rayon variant this constant has to be replaced by an ansatz of the form  $a/(b+v)$  ( $a$  and  $b$  are constant model parameters and  $v$  is the contraction speed). They demonstrate that the latter resembles the behavior of biological muscle, while the iron shell version leads to considerably more oscillations. They also criticize (Klute et al., 2002) for a misinterpretation of Hill's model. Again, none of the last three mentioned contributions consider hysteresis, although Toudu had used Coulomb terms in older papers.

(Davis and Caldwell, 2006) took on ideas from the already mentioned (Toudu and Lopez, 2000) and (Chou and Hannaford, 1994) concerning Coulomb friction to devise a very complex model of the braid's friction properties. Recently, (Minh et al., 2011) presented a more phenomenological Maxwell-slip model approach for single Festo MAS-20 muscles

and the same was done for an antagonistic joint in (Minh et al., 2010). They build on the rate-independence assumption from the research group around Hannaford and verify this assumption for the Festo muscle. While this result is somewhat surprising when compared to the Hill's model analogy previously found in (Kerscher et al., 2006) (who used exactly the same muscle type), it seems that the main reason for this discrepancy might be the different considered speed ranges. For rotational joints the arm transforms the muscle speed upwards to the tip. Therefore, lower muscle speeds than in linear applications are typically used in such setups. While Minh et al. use speeds of 1 mm/s and 16 mm/s to support their rate-independence assumption, the force/speed characteristic by Kerscher et al. presumably<sup>1</sup> ranges from 0 to 900 mm/s.

(Minh et al., 2009) is the only contribution we are aware of, where a hysteresis compensator is used in a pneumatic muscle position controller and the improvements are evaluated. (Boblan, 2009) provides some hysteresis modeling ideas for single Festo muscles and also mentions that they are very lightly damped. The lack of measurement data for the hysteresis behavior of the complete joint is given as a reason for neglecting it in the control scheme. Similarly, (Van Damme, 2009) develops a Preisach hysteresis model for pleated pneumatic artificial muscles but states that without knowledge of the initial hysteresis state the utilization in a controller is too cumbersome. Other recent publications on position control, for example (Aschemann and Schindele, 2008) or (Krichel et al., 2010) show a good controller performance without explicitly considering effects like hysteresis, damping or friction in their models.

Here, we want to evaluate the usefulness of a local compensator for the hysteresis in the joint angle for quasi-static pressure differences. In our approach we completely separate the nonlinear static characteristic and the hysteresis model.

Our joint hysteresis model is based on a Prandtl-Ishlinskii operator approach as described in (Kuhnen, 2003) for a magnetostrictive actuator. The nominal pressure difference for a certain joint angle under the zero load assumption, i.e.  $Q = 0$ , can be calculated from the static joint model as

$$\Delta p_{\text{nom}} = \frac{1}{B(q)} (-A(q) p_m - C(q)), \quad (1)$$

where  $p_m$  is the mean pressure and  $A$ ,  $B$  and  $C$  are polynomials that approximate pointwise, global (i.e.

<sup>1</sup>In the referred to Figure 11 no explanation of the used scaling value  $v_{\text{max}}$  is given, so this assumption is based on maximum speed values found in other plots.

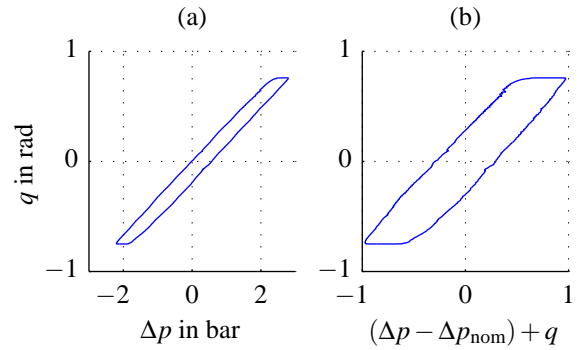


Figure 3: Hysteresis in the joint angle for slow variations of  $\Delta p$  (a). The nominal pressure difference was subtracted and as a purely mathematical procedure the joint angle was added to get a hysteresis loop around the 45° line (b).

over the whole pressure/torque/angle range), calibration measurements. Additionally, we applied a local calibration (i.e. for  $p_m = 3$  bar and  $Q = 0$ ) with a polynomial fit to really just extract the hysteresis cycle.

For the hysteresis parameter identification process we arranged the loop around the 45° line by adding the joint angle (in rad) to the difference between actual and nominal pressure differences (in bar) as shown in Figure 3.

For the hysteresis model we adopted the nomenclature used in (Kuhnen, 2003). The output signal,  $y$ , (which is  $q$  in our case) is directly the result of the Prandtl-Ishlinskii operator,

$$y = H[x] = \mathbf{w}_H^T \mathbf{H}_{r_H}[x, \mathbf{z}_{H0}], \quad (2)$$

which is a linear superposition, weighted by factors

$$\mathbf{w}_H = [w_{H,1} \ w_{H,2} \ \dots \ w_{H,N}]^T, \quad (3)$$

of  $N$  elementary so-called play-operators,

$$\mathbf{H}_{r_H}[x, \mathbf{z}_{H0}] = [H_{r_{H,1}}[x, z_{H0,1}] \ \dots]^T, \quad (4)$$

depending on the input signal,  $x$ , ( $\Delta p - \Delta p_{\text{nom}} + q$  for us) and the vector of initial internal states,

$$\mathbf{z}_{H0} = [z_{H0,1} \ z_{H0,2} \ \dots \ z_{H0,N}]^T. \quad (5)$$

Like the vector of weights, the vector of thresholds,

$$\mathbf{r}_H = [0 \ r_{H,2} \ \dots \ r_{H,N}]^T, \quad (6)$$

is a parameter of the model.

The play operator (see Figure 4),

$$z = H_{r_H}[x, z_{H0}], \quad (7)$$

is usually defined recursively as

$$z = H(x, z, r_H) \quad (8)$$

with the initial condition

$$z|_{t=0} = z_{H0} \quad (9)$$

and the threshold parameter  $r_H \in \mathbb{R}_0^+$ . Here,

$$H(x, z, r_H) = \max\{x - r_H, \min\{x + r_H, z\}\} \quad (10)$$

is the sliding, symmetrical dead-zone function. For a discrete time system, Equation 8 can be written as

$$z_k = H(x_k, z_{k-1}, r_H) \quad (11)$$

with the index  $k$  denoting the  $k$ -th sample of a signal.

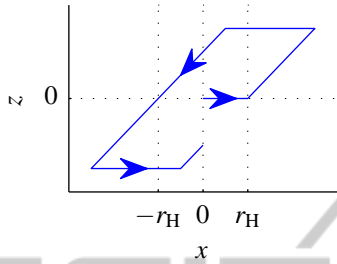


Figure 4: Example input/output trajectory of the play operator, starting at an initial position  $z = 0$ . Note, that the slope of the elementary operator is always 1.

To determine the parameters of the model,  $\mathbf{r}_H$ ,  $\mathbf{z}_{H0}$  and  $\mathbf{w}_H$ , we first select evenly spaced threshold values,

$$r_{H,i} = \frac{i-1}{N} \|x\|_\infty, \quad (12)$$

and initial states

$$z_{H0,i} = 0 \quad (13)$$

with  $i = 1..N$ . Then, the weights are calculated by minimizing

$$J = \int_{t_0}^{t_e} \|e\|^2 dt, \quad (14)$$

with the error

$$e = y - \mathbf{w}_H^T \mathbf{H}_{r_H}[x, \mathbf{z}_{H0}], \quad (15)$$

subject to the inequality constraint

$$\mathbf{w}_H \geq \begin{bmatrix} \varepsilon \\ 0 \\ \vdots \\ 0 \end{bmatrix}, \quad (16)$$

where  $\varepsilon$  is a positive, but arbitrarily small constant. The time  $t_0$  is the start and  $t_e$  the end time of the measured hysteresis cycle (see Figure 3) towards which the parameters are optimized.

For our application we chose  $N = 100$  and  $\varepsilon = 0.001$ . We solved the quadratic optimization problem, Equations 14 and 16 for our time discrete measurement data of  $x$  and  $y$  using the qpOASES package from (Ferreau et al., 2008). Of the 100 weights only 14 turned out to be non-zero. Consequently, the elementary play operators associated with the remaining weights were dropped for the final model.

The inequality constraint, Equation 16, guarantees an invertible model by limiting the slope of the hysteresis model to strictly positive values. The parameters of the inverse operator,

$$H^{-1}[y] = \mathbf{w}'_H{}^T \mathbf{H}_{r'_H}[y, \mathbf{z}'_{H0}], \quad (17)$$

can be calculated from

$$r'_{H,i} = \sum_{j=1}^i (w_{H,j} (r_{H,i} - w_{H,j})), \quad (18)$$

$$w'_{H,i} = \begin{cases} \frac{1}{w_{H,1}} & i = 1 \\ -\frac{w_{H,i}}{(\sum_{j=1}^i w_{H,j})(\sum_{j=1}^{i-1} w_{H,j})} & i = 2 \dots N \end{cases} \quad \text{and} \quad (19)$$

$$z'_{H0,i} = \sum_{j=1}^i w_{H,j} z_{H0,i} + \sum_{j=i+1}^N w_{H,j} z_{H0,j}. \quad (20)$$

Figure 5 shows a comparison of the inverse model – corrected by the previously added  $q$ -term – to the measurement data.

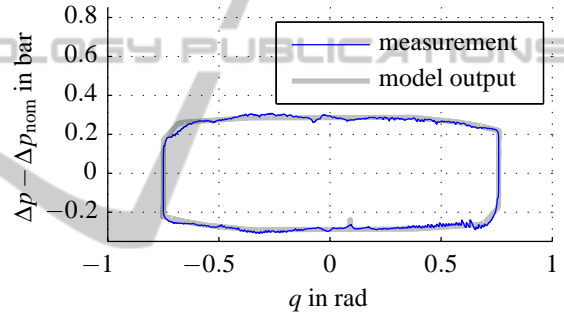


Figure 5: Inverse hysteresis model output compared to measurement data.

## 4 CONTROL

The implemented joint controllers (see Figure 6) use a cascaded structure with inner, flatness based, pressure control loops. The position controller uses a PID control law for feedback and additional feedforward action from the inverse dynamics. A linear, local joint observer estimates the states. It uses a nominal moment of inertia of the joint as model information in addition to an integral estimation of the remaining load torque components. A gain-scheduling anti-windup logic has been added. However, it becomes only active in case of fast and large disturbances, since our target trajectories are designed to obey the actuator flow and pressure limits.

The calculated pressure difference of the compensator is added to the output of the inv. joint characteristic. Note, that for the flatness based pressure control the time derivative of the desired pressure is required, which is generated by numerical differentiation.

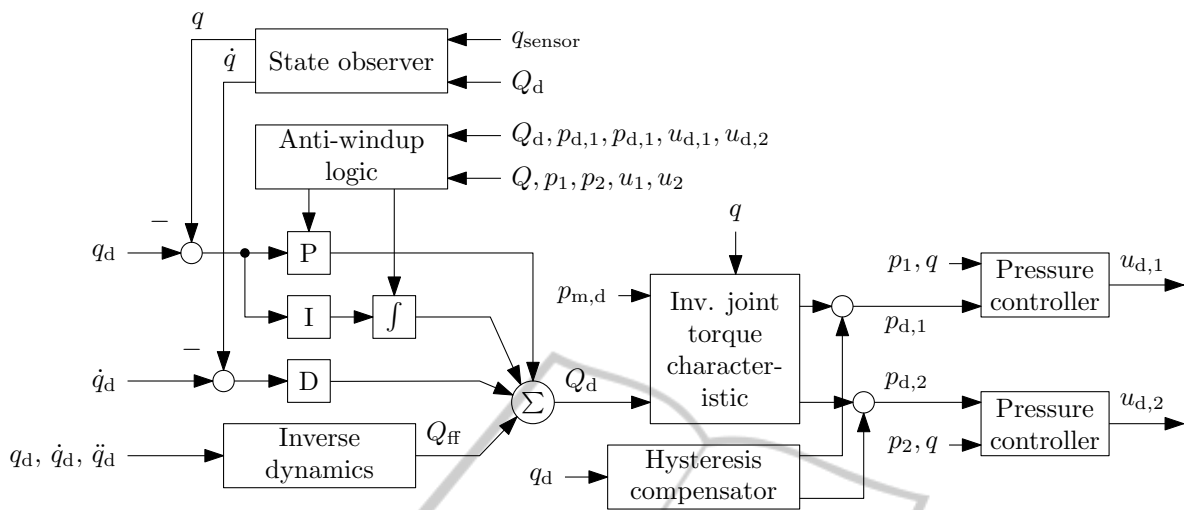


Figure 6: Implemented joint controller structure. Subscript d denotes desired values.

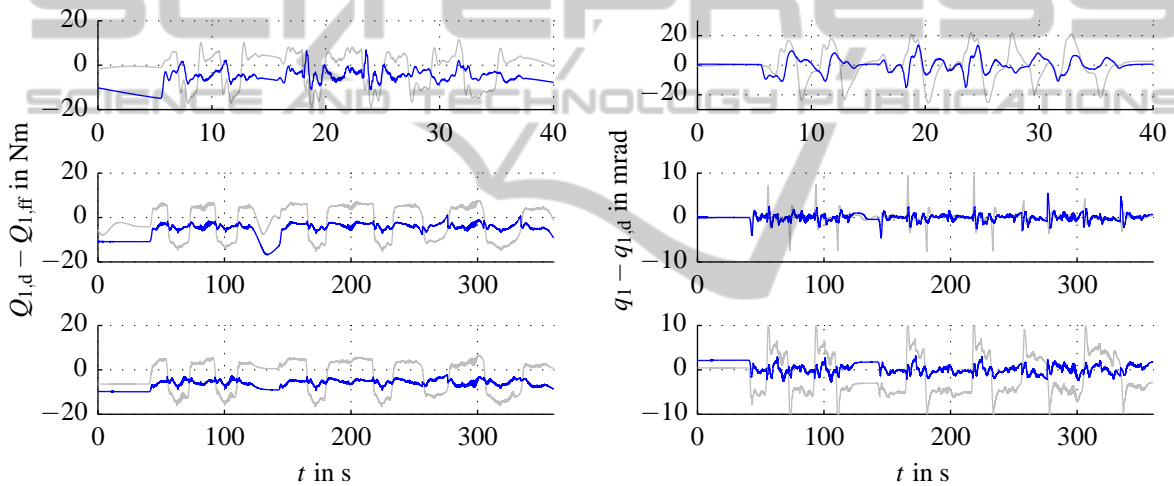


Figure 7: Evaluation results of the hysteresis compensator for the first joint of the Romo robot. Regular lines were taken with enabled and light lines with disabled hysteresis compensator. The first row is from the fast experiment while for the second a time scaling of 1/10 was used. In the third the integrator part of the position controller was disabled for the slow experiment.

## 5 EVALUATION

The evaluation of the control performance when using the hysteresis compensator in the first joint was done tracking a trajectory designed to the recommendations of the ISO 9283 norm (rounded rectangles, circles and lines in space) at different speeds. The results are shown in Figure 7. Especially in the slow trial there is a significant improvement in the control quality. An interesting observation is that there seems to be some interplay between the hysteresis compensation and the integrator part of the controller – see the difference in the torque errors at  $t = 130$ s where the first joint is at rest.

We have not yet created a hysteresis model for the

other two joints in the way described above. However, in these joints the feedback part is working much better than in the first joint (see Figure 8,  $q_1$  mainly influences the y direction – see Figure 1).

## 6 CONCLUSIONS

In this paper we discussed the advanced modeling of robot joints actuated by pneumatic muscles using hysteresis compensation. We evaluated the resulting compensator in the position controller of a robot, which led to promising results. In the future we want to look into the observed interplay between the inte-

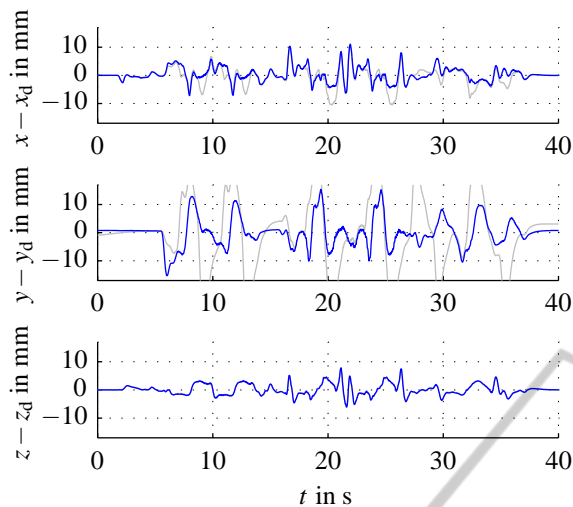


Figure 8: Tracking errors during the fast ISO 9283 test with (regular line) and without (light line) hysteresis compensation in the first joint.

grator part and the hysteresis compensator as well as devise models for the other joints. Furthermore, using the compensator in a disturbance force observer would be an interesting scenario.

## ACKNOWLEDGEMENTS

This work was supported by the Austrian Center of Competence in Mechatronics (ACCM) and the ODEUO project, an experiment funded in the context of the European Clearing House for Open Robotics Development (ECHORD) project.

## REFERENCES

- Aschemann, H. and Schindele, D. (2008). Sliding-mode control of a high-speed linear axis driven by pneumatic muscle actuators. *Industrial Electronics, IEEE Transactions on*, 55(11):3855–3864.
- Boblan, I. (2009). *Modellbildung und Regelung eines fluidischen Muskelpaares*. PhD thesis, Technical University Berlin.
- Chou, C.-P. and Hannaford, B. (1994). Static and dynamic characteristics of McKibben pneumatic artificial muscles. In *Robotics and Automation, 1994. Proceedings., 1994 IEEE International Conference on*, volume 1, pages 281–286.
- Davis, S. and Caldwell, D. G. (2006). Braid effects on contractile range and friction modeling in pneumatic muscle actuators. *The International Journal of Robotics Research*, 25(4):359–369.
- Ferreau, H., Bock, H., and Diehl, M. (2008). An online active set strategy to overcome the limitations of explicit MPC. *International Journal of Robust and Nonlinear Control*, 18(8):816–830.
- Hill, A. V. (1938). The heat of shortening and the dynamic constants of muscle. *Proceedings of the Royal Society of London. Series B, Biological Sciences*, 126(843):136–195.
- Kerscher, T., Albiez, J., Zöllner, J., and Dillmann, R. (2006). Evaluation of the dynamic model of fluidic muscles using quick-release. *First IEEE/RAS-EMBS International Conference on Biomedical Robotics and Biomechanics*.
- Klute, G. K., Czerniecki, J. M., and Hannaford, B. (2002). Artificial muscles: Actuators for biorobotic systems. *The International Journal of Robotics Research*, 21(4):295–309.
- Krichel, S., Sawodny, O., and Hildebrandt, A. (2010). Tracking control of a pneumatic muscle actuator using one servovalve. In *American Control Conference (ACC), 2010*, pages 4385–4390.
- Kuhnen, K. (2003). Modeling, identification and compensation of complex hysteretic nonlinearities: A modified Prandtl-Ishlinskii approach. *European Journal of Control*, 9:407–418.
- Minh, T., Tjahjowidodo, T., Ramon, H., and Van Brussel, H. (2009). Control of a pneumatic artificial muscle (PAM) with model-based hysteresis compensation. In *Advanced Intelligent Mechatronics, 2009. AIM 2009. IEEE/ASME International Conference on*, pages 1082–1087.
- Minh, T. V., Kamers, B., Tjahjowidodo, T., Ramon, H., and Van Brussel, H. (2010). Modeling torque-angle hysteresis in a pneumatic muscle manipulator. In *Advanced Intelligent Mechatronics (AIM), 2010 IEEE/ASME International Conference on*, pages 1122–1127.
- Minh, T. V., Tjahjowidodo, T., Ramon, H., and Van Brussel, H. (2011). A new approach to modeling hysteresis in a pneumatic artificial muscle using the Maxwell-slip model. *Mechatronics, IEEE/ASME Transactions on*, 16(1):177–186.
- Reynolds, D. B., Repperger, D. W., Phillips, C. A., and Bandry, G. (2003). Modeling the dynamic characteristics of pneumatic muscle. *Annals of Biomedical Engineering*, 31:310–317.
- Tondu, B. and Lopez, P. (2000). Modeling and control of McKibben artificial muscle robot actuators. *Control Systems, IEEE*, 20(2):15–38.
- Tondu, B. and Zagal, S. (2006). McKibben artificial muscle can be in accordance with the Hill skeletal muscle model. In *Biomedical Robotics and Biomechanics, 2006. BioRob 2006. The First IEEE/RAS-EMBS International Conference on*, pages 714–720.
- Van Damme, M. (2009). *Towards Safe Control of a Compliant Manipulator Powered by Pneumatic Muscles*. PhD thesis, Vrije Universiteit Brussel.